Reaction Time and Film Thickness Effects on Phase Formation and Optical Properties of Solution Processed Cu_2ZnSnS_4 Thin Films

Amna Safdar, Mohammad Islam, Muhammad Aftab Akram, Mohammad Mujahid, Yasir Khalid & S. Ismat Shah

Journal of Materials Engineering and Performance

ISSN 1059-9495

J. of Materi Eng and Perform
DOI 10.1007/s11665-015-1874-6

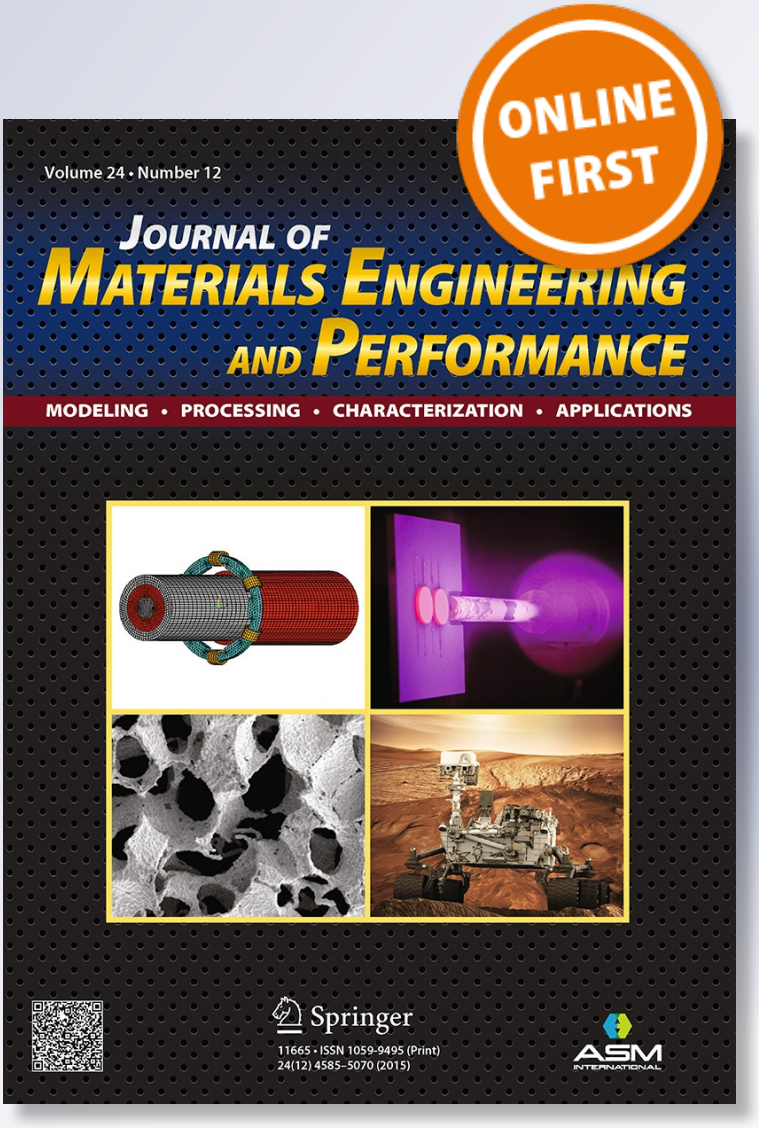

Springer

JMEPEG
DOI: 10.1007/s11665-015-1874-6

1059-9495/$19.00

Reaction Time and Film Thickness Effects on Phase Formation and Optical Properties of Solution Processed Cu_2ZnSnS_4 Thin Films

Amna Safdar, Mohammad Islam, Muhammad Aftab Akram, Mohammad Mujahid, Yasir Khalid, and S.Ismat Shah

(Submitted July 14, 2015; in revised form December 16, 2015)

Copper-zinc-tin-sulfide (Cu_2ZnSnS_4 or CZTS) is a promising p-type semiconductor material as absorber layer in thin film solar cells. The sulfides of copper and tin as well as zinc and sulfur powders were dissolved in hydrazine. The effect of chemical reaction between precursor species, at room temperature, was assessed for 6 to 22 h. For 22 h reaction time, the effect of spin coated film thickness on the resulting composition, after annealing under N_2 flow at 500 °C for 1 h, was investigated. The morphology, composition, and optical properties of the annealed films were determined by means of x-ray diffraction, scanning electron microscope, and spectrophotometer studies. It was found that, for less than optimal reaction time of 22 h or film thickness below 1.2 µm, other ternary phases namely Cu_4SnS_4, $Cu_5Sn_2S_7$, and ZnS co-exist in different proportions besides CZTS. Formation of phase-pure CZTS films also exhibited a tendency to minimize film cracking during annealing. Depending on the processing conditions, the band gap (E_g) values were determined to be in the range of 1.55 to 1.97 eV. For phase-pure annealed CZTS film, an increase in the E_g value may be attributed to quantum confinement effect due to small crystallite size.

Keywords band gap, Cu_2ZnSnS_4, kesterite, semiconductor, thin films

1. Introduction

I-III-VI_2 group-based compounds are *p*-type semiconductors with chalcopyrite crystal structure. The chemical composition $CuIn_xGa_{1-x}Se_2$, a solid solution of $CuInSe_2$ and $CuGaSe_2$, possesses very high absorption coefficient ($>10^5$ cm^{-1}) and the ability to tailor band gap energy value in the range of 1.0 to 1.7 eV. Incorporating $CuIn_xGa_{1-x}Se_2$ as an absorber layer in thin film solar cells, record power conversion efficiencies of 21.7 [1] and 16.5% [2], respectively, were reported for individual solar cells and a flexible module with 1.09 m^2 area. The issues of extensive use of In for LCD industry casting doubts on it future availability, high cost of Ga and hazardous nature of Se, however, have prompted exploration of alternative cost-effective, non-toxic compositions. For this purpose, chalcogenide compounds with general chemical formula, $Cu_2(M_{II})(M_{IV})(SSe)_4$, where M_{II} = Mn, Fe, Co, Ni, Zn, Cd, Hg, and M_{IV} = Si, Ge,Sn, are attractive due to their availability as naturally occurring minerals and direct band gap values. Among various stoichiometric compositions, the quaternary compound copper-zinc-tin-sulfide (Cu_2ZnSnS_4 or CZTS), has turned out to be a strong candidate as a cost-effective alternative replacing In, Ga, and Se by relatively inexpensive, more abundant and non-hazardous Zn Sn and S. CZTS is a p-type semiconductor with the cost of natural resources that is much less than those for CdTe, CIGSSe or Si (amorphous or polycrystalline)-based thin film PV technologies [3, 4].

CZTS has kesterite crystal structure with direct band gap energy in the range of 1.0 to 1.5 eV and high absorption coefficient of $\geq 10^4$ cm^{-1} [5-8]. CZTS films can be produced using both vacuum and solution-based processing techniques. Vacuum-assisted synthesis offers better process control and minimum contamination level with maximum reported efficiency of 6.67% [9, 10]. Liquid processing routes, on the other hand, offer cost-effective alternatives for commercialization, thus making them more attractive [11]. Synthesis of CZTS nanocrystals and thin films has been accomplished by devising various wet chemistry routes namely SILAR method [6], electrochemical deposition followed by sulfurization [12], colloidal synthesis [13], sol-gel sulfurization [14], spray pyrolysis [15], and hydrothermal technique [16]. Recent reports [17-20] have described a particle/solution hybrid approach involving use of both hydrazine and non-hydrazine solvents towards fabrication of CZTS-based solar cells with very high efficiencies.

Although initial research focused on vacuum processing of CZTS/CZTSe-based solar cells, non-vacuum-based techniques were also explored to assess solar cell device performance. CZTS incorporation into solar cells using sol-gel method, electrochemical deposition and solvothermal synthesis resulted in maximum efficiencies of 1.61 [21], 3.4 [22], and 5.9% [23], respectively. Record efficiency of 12.6% [24] was reported for a solar cell incorporating CZTSSe absorber layer fabricated through a hydrazine solution process. In a typical particle/solution hybrid approach, an appropriate choice of metal precursors

Amna Safdar, Muhammad Aftab Akram, and **Mohammad Mujahid**, School of Chemical and Materials Engineering (SCME), National University of Sciences and Technology, Islamabad 44000, Pakistan; **Mohammad Islam,** Deanship of Scientific Research, Advanced Manufacturing Institute, King Saud University, P. O. Box 800, Riyadh 11421, Saudi Arabia; **Yasir Khalid,** Institute of Energy Technologies, Universitat Politècnica de Catalunya, Diagonal 647, 08028 Barcelona, Spain; and **S. Ismat Shah,** Department of Physics and Astronomy and Department of Material Science and Engineering, University of Delaware, Newark, DE 19716, USA. Contact e-mails: mohammad.islam@gmail.com and miqureshi@ksu.edu.sa.

Published online: 04 January 2016

together with presence of particles in the solution facilitates wet processing by resolving the limited solubility issues of any particular chemical reagent, acting as an efficient binding medium, possibility to produce relatively thicker stress-free and crack-free layers and providing the intimate contact for rapid reactions, thus leading to homogeneous phase formation. Since this processing approach is relatively new, there are numerous process parameters that need to be investigated for their effect on the composition, shape, and morphology of the resulting product.

Among various processing parameters, the reaction time between precursor species is very critical towards formation of phase-pure CZTS composition. In this work, we present the effect of reaction time for a particle/solution mixture containing sulfides of copper and tin and zinc metal powder with Zn/Sn and Cu/(Zn + Sn) ratios (by mole) to be ~1.36. The film thickness values obtained from certain spin coating cycles is another variable whose effect was investigated. Both as-deposited and the annealed films were characterized for surface microstructure, composition, and optical properties.

2. Experimental

2.1 Thin Film Deposition

The chemicals used for this study were of analytical grade with 99.99% purity (Aldrich chemicals) and were used without any further treatment. Small coupons of sodalime glass (SLG), 25×25 mm^2 in size, were used as substrate. The substrates were ultrasonically cleaned in acetone and then rinsed with distilled water.

The experiment was carried out at room temperature (23 °C) in a glove-box under N_2 environment to avoid exposure to hydrazine. The solution was prepared by dissolving copper sulfide (CuS) and tin sulfide (SnS) in hydrazine (N_2H_4) in the presence of zinc metal (Zn) powder. The molar ratio of Cu:Zn:Sn:S was taken to be 0.90:0.38:0.28:2.0. The S content in the solution was maintained in excessive amount using S powder to compensate for its loss during annealing process. Theoretically, the Cu/(Zn + Sn) and Zn/Sn ratios were maintained at a value of 1.36. Complete dissolution of the CuS and SnS salts as well as Zn metal powder was ensured at room temperature by means of magnetic stirring at 350 rpm. The reaction time between various chemical species was varied from 6 to 22 h to investigate formation of different phases.

After desirable reaction times, the solution was spin cast over clean SLG substrates at 1200 rpm for 45 s. To ensure reasonable film thickness, the films were produced after five (5) spin coating cycles. The annealing treatment was carried out at 500 °C for 1 h under nitrogen flow. Using the solution obtained after 22 h reaction time, films with different thickness values

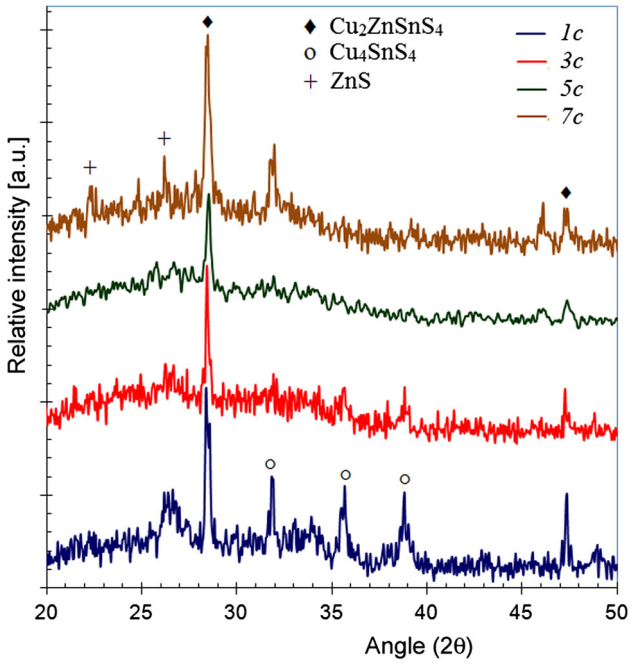

Fig. 1 X-ray diffraction patterns of the annealed CZTS films obtained after different spin cycles

Table 1 Identification scheme, processing conditions, and composition of the CZTS films

ID	Processing conditions	Thickness μm	Phase(s)	CZTS %	t (nm) (112)	EDS (at.%) Cu/(Zn + Sn)	EDS (at.%) Zn/Sn	%T	E_g (eV)
Spin Coating cycles 22 h, 1200 rpm, 45 s									
1.	1 cycle	0.97	○ Cu_4SnS_4 ♦ Cu_2ZnSnS_4			1.15	0.47		1.77 ± 0.04
2.	3 cycles	2.59	○ Cu_4SnS_4 ♦ Cu_2ZnSnS_4			1.03	0.87		1.78 ± 0.04
3.	5 cycles	3.33	♦ Cu_2ZnSnS_4			1.28	0.71		1.89 ± 0.05
4.	7 cycles	4.80	○ Cu_4SnS_4 ♦ Cu_2ZnSnS_4			1.10	0.55		1.97 ± 0.05
Reaction time 1200 rpm, 45 s, 5 cycles									
5	6 h	0.91	○ Cu_4SnS_4 ♦ Cu_2ZnSnS_4 • $Cu_5Sn_2S_7$	9.3	7.1, 15.9 59.9 514.8	1.23	0.46	43	1.55 ± 0.04
6.	12 h	1.54	○ Cu_4SnS_4 ♦ Cu_2ZnSnS_4 + ZnS	23.6	50.9, 63.3 32.5	1.02	0.88	64	1.61 ± 0.04
7.	18 h	2.41	♦ Cu_2ZnSnS_4 ○ Cu_4SnS_4	37.9	42.9 25.5, 29.5	0.72	1.27	75	1.66 ± 0.04
8.	22 h	3.53	♦ Cu_2ZnSnS_4	99.2	29.5	1.21	0.83	44	1.82 ± 0.05

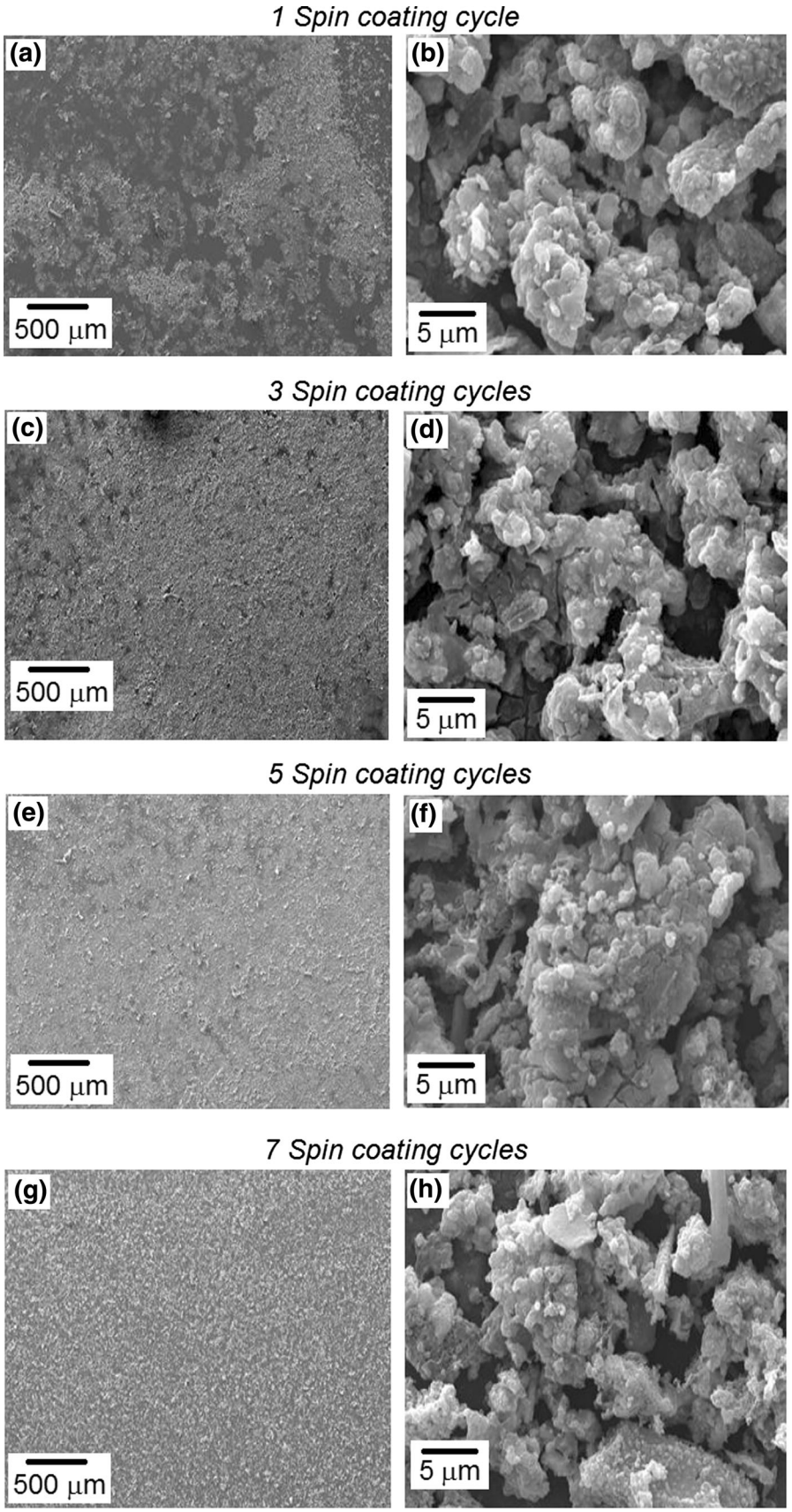

Fig. 2 Low and high magnification microstructures of the CZTS films produced after 22 h reaction time and from different spin coating cycles: (a, b) 1 cycle, (c, d) 3 cycles (e, f) 5 cycles, and (g, h) 7 cycles

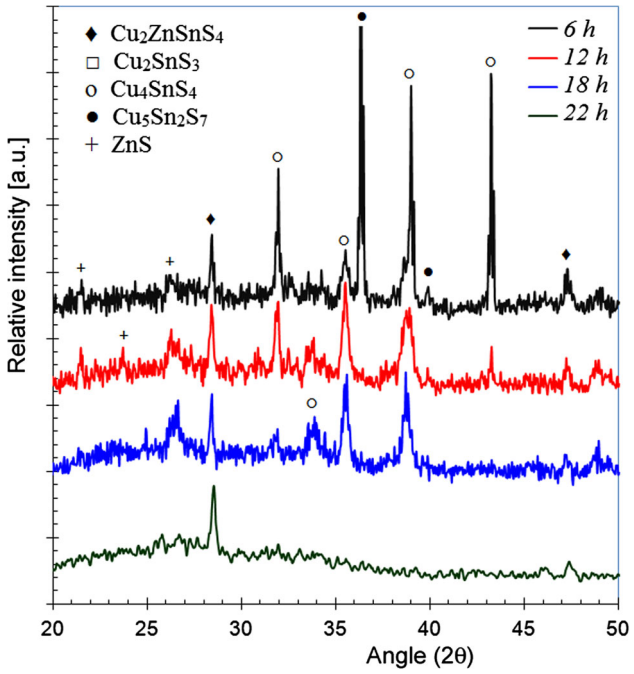

Fig. 3 X-ray diffraction patterns of the annealed CZTS films produced after different reaction times

for up to 7 spin coating cycles were produced and examined. Table 1 lists processing conditions and properties of the annealed CZTS films.

2.2 Characterization Studies

The crystalline quality and composition of the annealed films were determined from x-ray diffraction studies (XRD; STOE Stadi MP) using monochromatic CuKα radiation (1.5405 Å) at operating voltage and emission current values of 30 kV and 12 mA, respectively. The diffraction patterns were obtained for 2θ values in the 20° to 50° range with 0.01° step size and 2°/min scan rate. The crystallite size t for phases present was computed from Scherrer relation $t = 0.94\lambda / (\beta_{1/2} \cos\theta)$ where λ and $\beta_{1/2}$ are the wavelength of the Cu-Kα radiation and full-width-at-half-maximum (FWHM) of the diffraction peaks. For spherical particles, the shape factor is a constant with a value of 0.94.

The surface and cross-sectional morphology was examined under scanning electron microscope (SEM; JEOL JSM6409A) operating at 20 kV and field-emission transmission electron microscope (FE-TEM; JEOL JEM-2100F) with 300 kV accelerating voltage, LaB_6 electron gun and 0.18 nm point-to-point resolution. Energy dispersive spectrum (EDS) analysis using Oxford Instruments X-act detector was carried out over a large area and the composition was averaged using three sets of

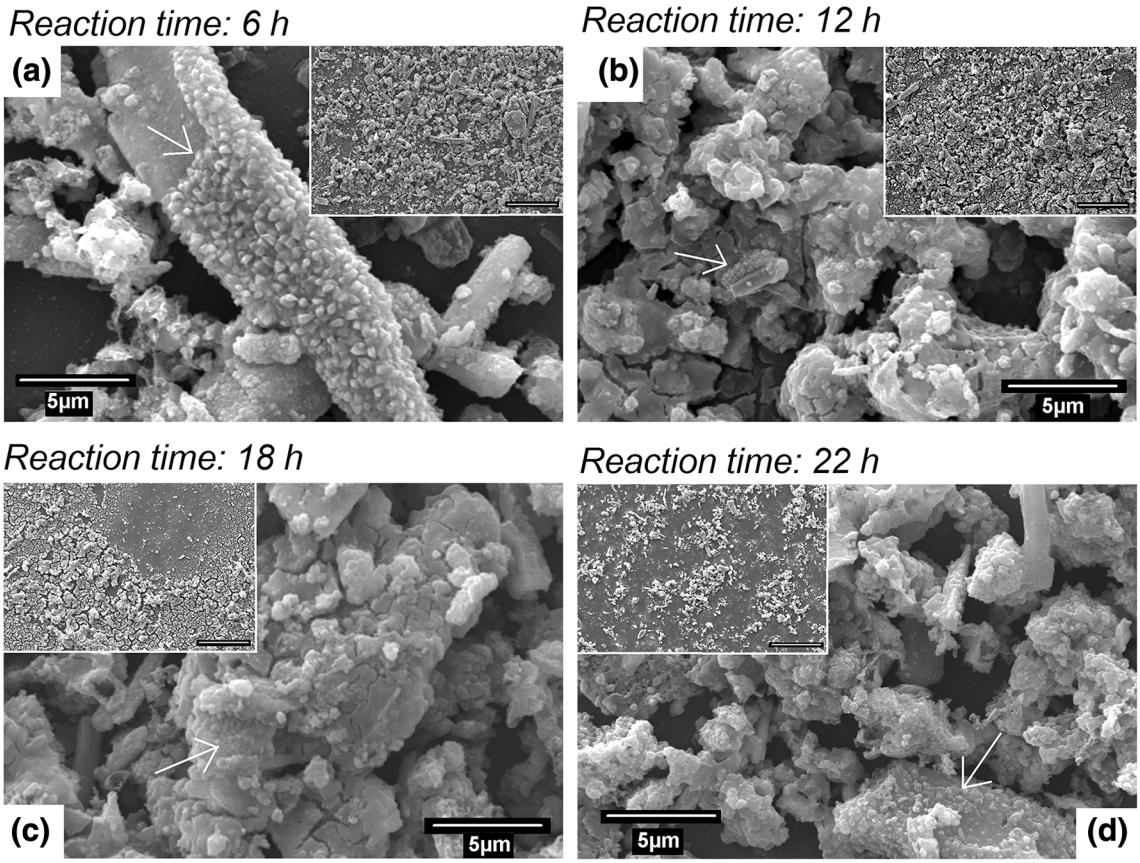

Fig. 4 SEM micrographs of the annealed CZTS films prepared from different reaction times: (a) 6 h, (b) 12 h, (c) 18 h, and (d) 22 h. The inset represents low magnification view and the scale-bar represents a length of 50 μm

measurements. The thickness values for the spin coated films were determined using an optical profilometer (Nanovea, PS20) as well as from SEM images of the film cross-sections.

The optical properties such as percent transmittance (%T) and band gap energy (E_g) values were measured using UV-vis spectrophotometer (Labomed UV2500). The optical absorption spectra were obtained at room temperature in the wavelength range of 200 to 1200 nm. The nature of direct optical inter-band transition was computed from Tauc plots using equation,

$$\alpha = \alpha_o(hv - E_g)/hv,$$

where α, *hv,* and E_g are respective values of the absorption coefficient, incident photon energy corresponding to a particular wavelength and the band gap energy.

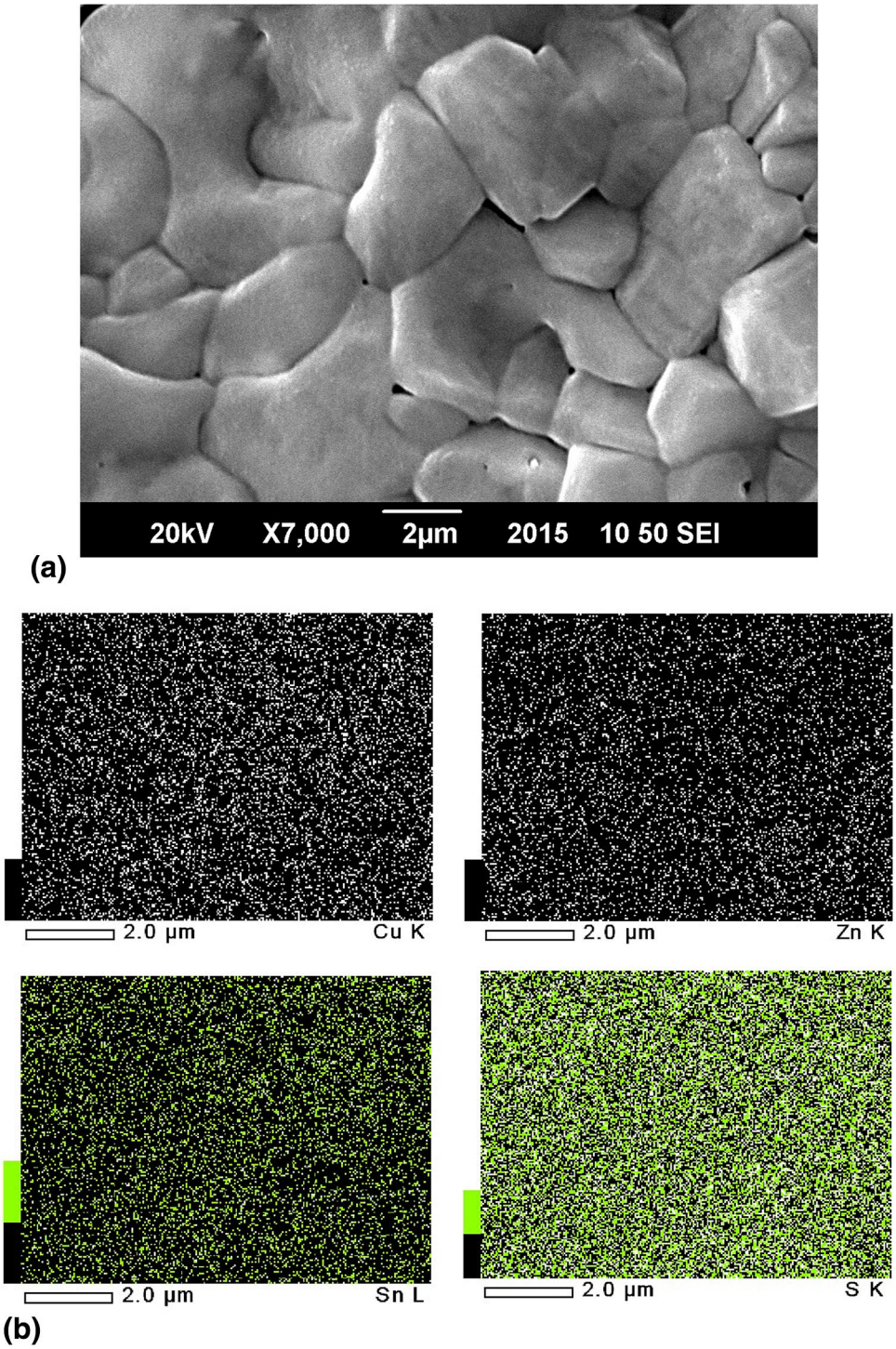

Fig. 5 The Annealed film produced from powder obtained after 22 h slurry reaction (sample 8, Table 1): (a) Low magnification SEM micrograph and (b) Elemental maps for the Cu, Zn, Sn, and S

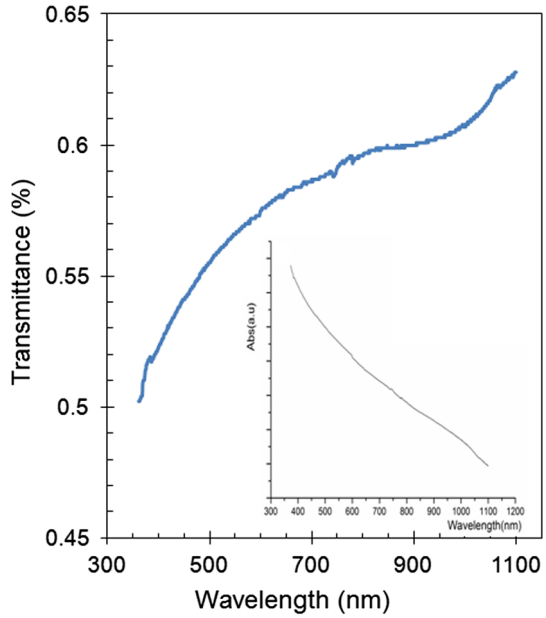

Fig. 6 The transmission spectrum of the CZTS film (sample 8, Table 1) with inset showing absorption coefficient as a function of wavelength

3. Results and Discussion

3.1 Effect of Spin Coating Cycles

The annealing temperature was optimized by investigating the effect of annealing temperature in the range of 480 to 560 °C. It was noticed that annealing at 560 °C causes loss of SnS to the vapor phase in a two-step reaction: solid SnS formation along with liberation of S vapors followed by SnS vaporization [25]. In some cases, SnS evaporation has been reported to occur at temperatures as low as 350 °C [26]. While annealing at 560 °C was noticed to induce a drastic change in surface morphology due to formation and evaporation of some low temperature volatile phase(s) with residual porosity, the annealing at 540 °C was also found to be in close proximity to the CZTS decomposition temperature. Although no significant difference in film surface morphology was seen upon annealing at 480 and 500 °C, an optimal value of 500 °C was chosen for further experimentation to avoid Sn loss as well as CZTS phase decomposition. Therefore, after 22 h reaction between precursor species at room temperature, the films with different thicknesses were produced from up to seven spin coating cycles and subsequently annealed at 500 °C for 1 h. The x-ray diffraction patterns of the resulting films are presented in Fig. 1. The XRD results reveal presence of a diffraction peak at 28.52° with maximum relative intensity which can be assigned to the (112) plane of the CZTS structure. For both single and seven spin coating cycles, coexistence of Cu_4SnS_4 phase is also noticed through peaks located at 35.6° and 38.8° besides diffraction peaks characteristic of hexagonal ZnS structure. The surface morphologies of the annealed films at low and high magnifications are shown in Fig. 2. For single spin coating cycle, two distinct regions comprising smooth (appears dark) and rough morphologies are seen. For multiple spin cycles, the film surfaces exhibit homogeneous coverage with rough granular deposits which, at high magnification, are found to be clusters made up of fine particles along with surface pores. Among the four different samples, film prepared from five spin coating cycles indicate relatively more dense morphology and less porosity level.

For 22 h reaction time between precursor reagents, the film thickness progressively increases from <1 μm to few micrometers upon increasing the number of spin coating cycles from 1 to 7. The samples 3 and 8, prepared under identical processing conditions, exhibit thickness values in close proximity to each other (Table 1). An increase in the reaction time (from 6 to 22 h) results in an associated increase in the film thickness for same number of spin coating cycles, implying that longer reaction times produce more homogeneous deposit at greater deposition rate.

3.2 Effect of Reaction Time

To investigate the effect of slurry reaction time on formation of different phases, films of same thickness values were prepared after slurry reaction times of 6, 12, 18, and 22 h via five spin coating cycles and annealing at 500 °C for 1 h. The XRD patterns presented in Fig. 3 show that after 6 h reaction time, Cu_4SnS_4 and $Cu_5Sn_2S_7$ were the predominantly formed phases as evident from presence of the diffraction peaks. As the reaction time was increased from 6 to 22 h, the overall composition of the films changed from multiphase i.e., different mixed sulfides of Cu, Sn, and/or Zn to phase-pure CZTS. The diffraction peaks positioned at 2θ values of 28.52° and 47.64° can be assigned to (112) and (220) planes of CZTS tetragonal structure (JCPDS 26-0575) [20]. While the peak at 28.52° is weak with relatively low intensity, it gradually becomes more intense as the precursor chemicals in the slurry are allowed prolonged reaction time. The other phases, that are present for low reaction times and diminish as the time is increased, are $Cu_5Sn_2S_7$ (JCPDS 40-0924), Cu_4SnS_4 (JCPDS 29-0584), and ZnS (JCPDS 89-2422).

To assess the reaction time effect on crystallite size (t) of various phases formed, the crystallite size of the CZTS phase was calculated using Scherrer equation. From (112) diffraction peak, the t values were found to be in the range of 29.5 to 59.9 nm. The maximum value of 59.9 nm for the film produced after 6 h reaction time cannot be attributed to the CZTS phase due to overlap in peak positions for the CZTS and Cu_2SnS_3 phases. Among other reaction times, while the crystallite size value for the CZTS phase maximizes for 18 h reaction time, the reduction in size for 22 h reaction time may be caused by transformation of other phases to CZTS phase for extended reaction time between precursor species. For 6 h reaction time, the crystallite size of the $Cu_5Sn_2S_7$ phase was ~515 nm which completely disappears upon increasing reaction time. On the other hand, the Cu_4SnS_4 phase shows an initial increase in crystallite size from 7 to 51 nm followed by a decrease to 26 nm upon increasing the reaction time to 12 and 18 h. For 12 h mixing, ZnS phase is found to co-exist with other phases, as indicated by the weak peak at 21.52°. Thus, among different reaction times investigated, the reaction time of 22 h was found to promote formation of phase-pure CZTS structure. It is noteworthy, however, that Scherrer equation only yields a lower bound on the particle size with several factors besides crystal size, namely instrument broadening, microstrain arising from different lattice defects and non-homogenous solid solution. In our case, the error margin in the calculated values must not exceed 5% of an individual value.

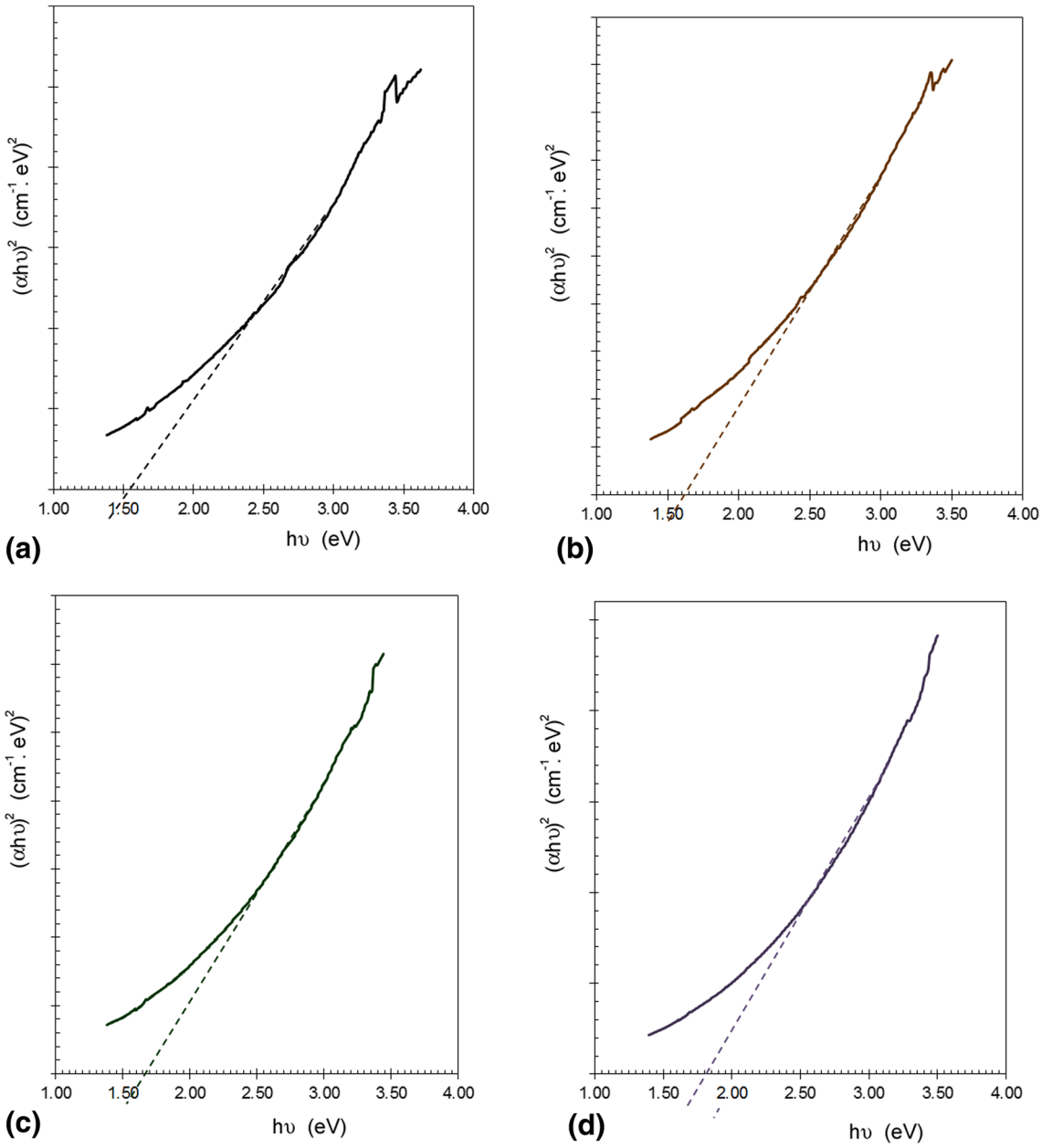

Fig. 7 Tauc plots for the annealed films (500 °C, 1 h) after different reaction times between precursor reagents (samples 5–8, Table 1)

Microstructural examination at low (inset) and high magnification, shown in Fig. 4, indicates presence of rough, granular microstructure over a relatively smooth surface. At high magnification, large particles with a change in apparent surface morphology can be seen (white arrows) which is indicative of chemical interaction between precursor species during reaction and afterwards during annealing treatment. The size of such features is in the range of ~350 to 550 nm and progressively becomes finer upon increasing the reaction time. For reaction times of 12 and 18 h, some degree of cracking is also evident in the microstructures, presented in Fig. 4(b, c), presumably due to solvent removal during the initial phase of annealing and film consolidation at elevated temperatures during annealing.

For sufficiently prolonged reaction time of 22 h, the films become Cu-poor, as indicated by the Cu/(Zn + Sn) values in Table 1. The presence of binary or ternary compositions, if any, is believed to be in an extremely small fraction that cannot be detected from XRD analysis. A low magnification microstructure of the sample 8 (Table 1) with elemental maps for Cu, Zn, Sn, and S are shown in Fig. 5. The results indicate homogeneous distribution of the constituent elements throughout the microscopic area selected for mapping.

3.3 Optical Properties

The transmittance spectrum of the sample 4 in the wavelength range of 200 to 1100 nm is shown in Fig. 6. The

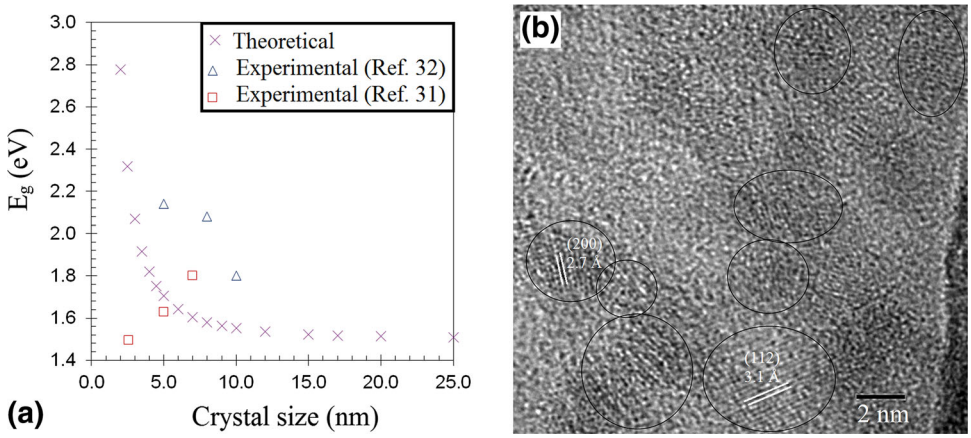

Fig. 8 (a) Graphical presentation of band gap energy (E_g) dependence on the crystallite size and (b) High resolution TEM microstructure of few nanoparticles from annealed powder after 22 h reaction time

transmittance values are in the range of 0.50 to 0.62 with value of the absorption coefficient to be $>10^4$ cm^{-1} as calculated using the relation $\alpha = (1/d)\ln[(1-R^2)/T]$, where R is the reflectance at the surface, d is the film thickness and T is the transmittance. Since the reaction is allowed to occur at room temperature, longer reaction times promote the presence of relatively more broad absorption at wavelengths of >500 nm beside the presence of CuS phase in the films [27-29].

The band gap energy values as determined from Tauc plots (Fig. 7) are listed in Table 1. The degree of uncertainty in the estimated values is caused by errors in determining the slope of the straight line and the x-intercept. From comparison of the values obtained, it is found that with an increase in the reaction time from 6 to 22 h, the E_g values increase from 1.55 to 1.82 eV. For low reaction times, presence of other ternary phases such as Cu_4SnS_4 ($E_g \sim 1.5$ eV), $Cu_5Sn_2S_7$ (E_g 1.45 eV) beside Cu_2ZnSnS_4 yields an overall low value of the band gap energy. Up to 18 h reaction time, the increase in the E_g value can be attributed to some degree of ZnS phase formation and indirect transition in Cu_4SnS_4 phase (E_g 1.61 to 1.84 eV) whereas the higher value obtained for 22 h time is attributed to quantum confinement effect in the CZTS nanoparticles. The fact that Cu_2SnS_3 phase has a relatively low value of E_g (~0.93 eV) confirms that this phase does not exist [14].

Although quantum confinement effect is more pronounced once the crystallite size is reduced below 10 nm, it is believed that a significant fraction of nanoparticles in that size range may be present in our films (samples 5, 8), thus inducing this increase in the band gap energy value. A comparison of the E_g values as a function of crystal size, as predicted theoretically using bulk CZTS E_g (1.50 eV), Bohr exciton radius (a_B = 4.3 nm) and exciton energy (E_b = 28 meV) [30] in the expression $E(t) = E(\infty) + E_b(\pi\ a_B/t)^2$ and the experimentally estimated E_g values by different groups is made in Fig. 8a. In contrast with studies that report particle size control using oleylamine as a capping agent [31, 32], our work is believed to produce nanoparticles with broad size range along with significant proportion of ultrafine nanoparticles. The synthesis conditions including solution chemistry, temperature, and reaction time affect the nanostructure size with prolonged reaction times usually leading to an increase in the crystallite size with subsequent diminishing of the quantum confinement effect. In our case, however, a relatively longer reaction time of 22 h is anticipated to be optimum for phase-pure CZTS formation, eliminating presence of other undesirable phases. The high resolution transmission electron microscope image, presented in Fig. 8b, shows few individual ultrafine spherical nanoparticles after annealing of the powder after 22 h reaction time between precursor chemicals. The particles are 2 to 5 nm in size and the lattice fringes exhibit inter-planar spacing values that correspond to the CZTS phase.

4. Conclusions

The processing parameters such as reaction time and film thickness govern phase composition in the annealed films prepared from hybrid particle/solution slurry containing zinc and sulfur and sulfides of copper and tin. Among the range of synthesis conditions explored, a reaction time of 22 h between precursor species and a coating thickness of ~1.4 μm were found to yield phase-pure CZTS composition. Increasing the reaction time from 6 to 22 h progressively reduces the fraction of compositions other than CZTS, as indicated by x-ray diffraction data and crystallite size measurements. Also, elimination of other undesirable phases upon annealing minimizes film cracking during annealing. The optical band gap values indicated a gradual increase with an increase in the solution mixture reaction time or greater thickness of the films produced after 22 h reaction time.

Acknowledgments

The work has been funded by the Higher Education Commission (HEC), Pakistan through the National Research Program for Universities (Grant No. 20-1603). The authors would like to extend their sincere appreciation to the Deanship of Scientific Research at King Saud University for its funding of this research through the Research Group Project no. RGP-VPP-283.

References

1. PV Magazine, ZSW sets 21.7% thin film efficiency record, http://www.pv-magazine.com/news/details/beitrag/zsw-sets-217-thin-film-efficiency-record_100016505/#axzz3NAQ5uFEp, 22 Sep 2014

2. PV Magazine, Thin-film competition hots up as TSMC Solar breaks day-old CIGS efficiency record, http://www.pv-tech.org/news/thin_film_competition_hots_up_as_tsmc_producer_breaks_day_old_cigs_efficien, 28 April, 2015
3. S. Siebentritt and A.S. Schorr, Kesterites—A Challenging Material for Solar Cells, *Prog. Poovoltaics*, 2012, **20**, p 512–519
4. M. Jiang, Yan X, Cu_2ZnSnS_4 Thin Film Solar Cells: Present Status and Future Prospects. In: Arturo Morales-Acevedo (Ed.) *Solar Cells—Research and Application Perspectives*, InTech (2013)
5. I.V. Fisher, S.R. Cohen, A. Ruzin, and D. Cahen, How Polycrystalline Devices Can Outperform Single-Crystal Ones Thin Film CdTe/CdS Solar Cells, *Adv. Mater.*, 2004, **16**, p 879–883
6. L. Arora, V.N. Singh, G. Partheepan, T.D. Senguttuvan, and K. Jain, One-Step Synthesis of Size-Controlled CZTS Quantum Dots, *Appl. Nanosci.*, 2015, doi:10.1007/s13204-015-0404-z (Feb 13)
7. D.-C. Nguyen, S. Ito, and D.V.A. Dung, Effects of Annealing Conditions on Crystallization of the CZTS Absorber and Photovoltaic Properties of Cu(Zn, Sn)(S, Se)2 Solar Cells, *J. Alloys Compd.*, 2015, **632**, p 676–680
8. R. Schurr, A. Hölzing, S. Jost, R. Hock, T. Voβ, J. Schulze, A. Kirbs, A. Ennaoui, M.L. Steiner, A. Weber et al., The Crystallisation of Cu2ZnSnS4 Thin Film Solar Cell Absorbers from Co-Electroplated Cu-Zn-Sn Precursors, *Thin Solid Films*, 2009, **517**(7), p 2465–2468
9. T. Todorov, O. Gunawan, S.J. Chey, T.G. de Monsabert, A. Prabhakar, and D.B. Mitzi, Progress Towards Marketable Earth-Abundant Chalcogenide Solar Cells, *Thin Solid Films*, 2011, **519**(21), p 7378–7381
10. K. Hironori, J. Kazuo, Y. Satoru, K.T.M.W. Shwe, F. Tatsuo, I. Tadashi, and M. Tomoyoshi, Enhanced Conversion Efficiencies of Cu_2ZnSnS_4-Based Thin Film Solar Cells by Using Preferential Etching Technique, *Appl. Phys. Express*, 2008, **1**(4), p 041201
11. A. Shavel, J. Arbiol, and A. Cabot, Synthesis of Quaternary Chalcogenide Nanocrystals: Stannite $Cu_2Zn_xSn_ySe_{1+x+2y}$, *J. Am. Chem. Soc.*, 2010, **132**(1), p 4414–4415
12. H. Wang, Progress in Thin Film Solar Cells Based on Cu_2ZnSnS_4, *Int. J. Photoenergy*, 2011, **2011**, p 1–10
13. G. Ma, T. Minegishi, D. Yokoyama, J. Kubota, and K. Domen, Photoelectrochemical Hydrogen Production on Cu_2ZnSnS_4/Mo-Mesh Thin-Film Electrodes prEpared by Electroplating, *Chem. Phys. Lett.*, 2011, **501**(4–6), p 619–622
14. S.C. Riha, B.A. Parkinson, and A.L. Prieto, Solution-Based Synthesis and Characterization of Cu_2ZnSnS_4 Nanocrystals, *J. Am. Chem. Soc.*, 2009, **131**(34), p 12054–12055
15. K. Tanaka, Y. Fukui, N. Moritake, and H. Uchiki, Chemical Composition Dependence of Morphological and Optical Properties of Cu_2ZnSnS_4 Thin Films Deposited By Sol-Gel Sulfurization and Cu_2ZnSnS_4 Thin Film Solar Cell Efficiency, *Solar Energy Mater. Solar Cells*, 2011, **95**(3), p 838–842
16. N. Nakayama and K. Ito, Sprayed Films of Stannite Cu_2ZnSnS_4, *Appl. Surf. Sci.*, 1996, **92**, p 5
17. M. Cao and Y. Shen, A Mild Solvothermal Route to Kesterite Quaternary Cu_2ZnSnS_4 Nanoparticles, *J. Cryst. Growth*, 2011, **318**, p 4
18. T.K. Todorov, K.B. Reuter, and D.B. Mitzi, High-Efficiency Solar Cell with Earth-Abundant Liquid-Processed Absorber, *Adv. Mater.*, 2010, **22**(20), p E156–159
19. D.B. Mitzi, M. Yuan, W. Liu, A.J. Kellock, S.J. Chey, L. Gignac, and A.G. Schrott, Hydrazine-Based Deposition Route for Device-Quality CIGS Films, *Thin Solid Films*, 2009, **517**(7), p 2158–2162
20. W.-C. Hsu, B. Bob, W. Yang, C.-H. Chung, and Y. Yang, Reaction Pathways for the Formation of Cu2ZnSn(Se, S)4 Absorber Materials from Liquid-Phase Hydrazine-Based Precursor Inks, *Energy Environ. Sci.*, 2012, **5**(9), p 8564
21. N. Moritake, Y. Fukui, M. Oonuki, K. Tanaka, and H. Uchiki, Preparation of Cu_2ZnSnS_4 Thin Film Solar Cells Under Non-vacuum Condition, *Phys. Status Solidi C*, 2009, **6**, p 1233–1236
22. A. Ennaoui, M. Lux-Steiner, A. Weber, D. Abou-Ras, I. Kotschau, H.-W. Schock, R. Schurr, A. Holzing, S. Jost, R. Hock, T. Voß, J. Schulze, and A. Kirbs, Cu_2ZnSnS_4 thin Film Solar Cells from Electroplated Precursors: Novel Low-Cost Perspective, *Thin Solid Films*, 2009, **517**, p 2511–2514
23. K. Timmo, M. Altosaar, J. Raudoja, K. Muska, M. Pilvet, M. Kauk, T. Varema, M. Danilson, O. Volobujeva, and E. Mellikov, Sulfur-Containing Cu2ZnSnSe4 Monograin Powders for Solar Cells, *Sol. Energy Mater. Sol. Cells.*, 2010, **94**, p 1889–1892
24. W. Wang, M.T. Winkler, O. Gunawan, T. Gokmen, T.K. Todorov, Y. Zhu, and D.B. Mitzi, Device Characteristics of CZTSSe Thin-Film Solar Cells with 12.6% Efficiency, *Adv. Energy Mater.*, 2014, **4**, p 1301465
25. J.J. Scragg, T. Ericson, T. Kubart, M. Edoff, and C. Platzer-Björkman, Chemical Insights into the Instability of Cu_2ZnSnS_4 Films during Annealing, *Chem. Mater.*, 2011, **23**, p 4625–4633
26. A. Weber, R. Mainz, and H.W. Schock, On the Sn Loss from Thin Films of the Material System Cu-Zn-Sn-S in High Vacuum, *J. Appl. Phys.*, 2010, **107**, p 013516
27. E.J. Silvester, F. Grieser, B.A. Sexton, and T.W. Healy, Spectroscopic Studies on Copper Sulfide Sols, *Langmuir*, 1991, **7**, p 2917–2922
28. S.K. Haram, A.R. Mahadeshwar, and S.G. Dixit, Synthesis and Characterization of Copper Sulfide Nanoparticles in Triton-X 100 Water-in-Oil Microemulsions, *J. Phys. Chem.*, 1996, **100**, p 5868–5873
29. T. Kameyama, T. Osaki, K. Okazaki, T. Shibayama, A. Kudo, S. Kuwabatade, and T. Torimoto, Preparation and Photoelectrochemical Properties of Densely Immobilized Cu_2ZnSnS_4 Nanoparticle Films, *J. Mater. Chem.*, 2010, **20**, p 5319–5324
30. F.-J. Fan, L. Wu, M. Gong, G. Liu, Y.-X. Wang, S.-H. Yu, S. Chen, L.-W. Wang, and X.-G. Gong, Composition- and Band-Gap-Tunable Synthesis of Wurtzite-Derived $Cu_2ZnSn(S_{1-x}Se_x)_4$ Nanocrystals: Theoretical and Experimental Insights, *ACS Nano*, 2013, **7**(2), p 1454–1463
31. A. Khare, A.W. Wills, L.M. Ammerman, D.J. Norrisz, and E.S. Aydil, Size Control and Quantum Confinement in Cu_2ZnSnS_4 Nanocrystals, *Chem. Commun.*, 2011, **47**, p 11721–11723
32. L. Arora, V.N. Singh, G. Partheepan, T.D. Senguttuvan and K. Jain, One-Step Synthesis of Size-Controlled CZTS Quantum Dots. Appl. Nanosci. doi:10.1007/s13204-015-0404-z